

PCCP

Accepted Manuscript

This article can be cited before page numbers have been issued, to do this please use: M. Brouard, S. D.S. Gordon, B. Nichols, V. Walpole, F. J. Aoiz and S. Stolte, *Phys. Chem. Chem. Phys.*, 2018, DOI: 10.1039/C8CP06225K.



This is an Accepted Manuscript, which has been through the Royal Society of Chemistry peer review process and has been accepted for publication.

Accepted Manuscripts are published online shortly after acceptance, before technical editing, formatting and proof reading. Using this free service, authors can make their results available to the community, in citable form, before we publish the edited article. We will replace this Accepted Manuscript with the edited and formatted Advance Article as soon as it is available.

You can find more information about Accepted Manuscripts in the [author guidelines](#).

Please note that technical editing may introduce minor changes to the text and/or graphics, which may alter content. The journal's standard [Terms & Conditions](#) and the ethical guidelines, outlined in our [author and reviewer resource centre](#), still apply. In no event shall the Royal Society of Chemistry be held responsible for any errors or omissions in this Accepted Manuscript or any consequences arising from the use of any information it contains.

Differential steric effects in the inelastic scattering of NO(X) + Ar: spin-orbit changing transitions.

M. Brouard,^{1, a)} S.D.S. Gordon,^{1, b)} B. Nichols,^{1, c)} V. Walpole,¹ F.J. Aoiz,^{2, d)} and S. Stolte^{3, e)}

¹⁾ *The Department of Chemistry, University of Oxford, Chemistry Research Laboratory, 12 Mansfield Rd, Oxford OX1 3TA*

²⁾ *Departamento de Química Física, Facultad de Química, Universidad Complutense, 28040 Madrid, Spain*

³⁾ *The Jilin Institute of Atomic and Molecular Physics, Qianjin Avenue, Changchung, 130012, China^{f)}*

(Dated: 3 November 2018)

Spin-orbit changing transitions for bond-axis oriented collisions of NO(X) with Ar have been investigated with full quantum state selection *via* a crossed molecular beam experiment at collision energies of 532 cm⁻¹ and 651 cm⁻¹. NO(X) molecules were selected in their ground rotational state ($\Omega = 0.5$, $j = 0.5$, f) before being adiabatically oriented using a static electric field, such that either the N- or O-end of the molecule was directed towards the incoming Ar atom. After collision, NO(X, $\Omega' = 1.5$, j' , e) molecules were probed quantum state specifically using velocity-map ion imaging, coupled with resonantly enhanced multi-photon ionization. Differences were observed between the experimental ion images and differential cross sections for collisions occurring at the two ends of the molecule, with results that could largely be accounted for by quantum mechanical scattering calculations. The bond-axis oriented data for the spin-orbit changing collisions are compared with similar results obtained previously for spin-orbit conserving transitions, and for field free scattering of NO(X) with Ar.

^{a)}Electronic mail: mark.brouard@chem.ox.ac.uk

^{b)}Current address: Institute for Chemical Sciences and Engineering, Ecole Polytechnique Fédérale de Lausanne, 1015 Lausanne, Switzerland

^{c)}Current address: The Department of Chemistry, University of California, Berkeley, California 94720, USA.

^{d)}Electronic mail: aoiz@quim.ucm.es

^{e)}Electronic mail: stolte@chem.vu.nl

^{f)}Department of Physics and Astronomy, LaserLaB, Vrije Universiteit, Amsterdam, De Boelelaan 1081, 1081 HV Amsterdam, The Netherlands

I. INTRODUCTION

Studies of scattering with oriented molecules are concerned with understanding the $\mathbf{k} - \mathbf{r} - \mathbf{k}'$ three-vector correlation between the initial and final relative velocities of the collision system, \mathbf{k} and \mathbf{k}' , and the initial orientation of the bond- or symmetry-axis of the molecular collider, \mathbf{r} , *i.e.* with the measurement of the angular distributions resulting from inelastic scattering for a defined bond- or symmetry-axis orientation.¹⁻³ Alongside the *integral steric asymmetry* – the two-vector $\mathbf{k} - \mathbf{r}$ correlation – the measurement of the three-vector correlation, the *differential steric asymmetry*, provides insight into the fundamental collision dynamics of the system, and allows information to be gained about differences in scattering arising from different collision geometries.¹⁻³

In the present work we focus on the measurement of steric effects in the inelastic scattering of NO(X) by Ar, in particular for the spin-orbit (SO) changing collisions in this system. The scattering of NO has been of considerable interest due to the open-shell character of its ground electronic state, which has a $^2\Pi$ term arising from an electronic configuration with a single unpaired electron in a π^* orbital. The NO($X^2\Pi$) state is split into two SO states, separated by $\sim 123 \text{ cm}^{-1}$; ⁴ $\Omega = 0.5$ (the ground SO state) and $\Omega = 1.5$ (the excited SO state), where Ω is the quantum number for the absolute value of the projection of the electronic angular momentum along the internuclear axis. In addition to the SO splitting, each rotational level, j , is split into two nearly degenerate Λ -doublet levels ($\epsilon = \pm 1, e/f$), which differ by parity, $p = \epsilon(-1)^{j-1/2}$.

The interaction of the NO(X) molecule with a closed-shell atom gives rise to two potential energy surfaces (PESs) defined by their symmetry ($V_{A'}$ and $V_{A''}$) depending on the orientation of the π^* orbital relative to the plane of approach of the atom. As shown by Alexander,⁵ for pure Hund's case (a) molecules, which is a reasonable approximation for low rotational states of NO(X), SO conserving ($\Delta\Omega = 0$) and changing ($\Delta\Omega = +1$) transitions may be considered to occur on the half-sum (V_{sum}) and half-difference (V_{diff}) potentials, respectively,

$$V_{\text{sum}} = \frac{1}{2} [V_{A''}(R, \gamma) + V_{A'}(R, \gamma)] = \sum_{\lambda} V_{\lambda 0}(R) d_{00}^{\lambda}(\gamma), \quad (1)$$

$$V_{\text{diff}} = \frac{1}{2} [V_{A''}(R, \gamma) - V_{A'}(R, \gamma)] = \sum_{\lambda} V_{\lambda 2}(R) d_{20}^{\lambda}(\gamma), \quad (2)$$

where $d_{mn}^{\lambda}(\gamma)$ are reduced Wigner rotation matrix elements, and $V_{\lambda m}(R)$ are radially depen-

dent expansion coefficients. R is the distance between the center-of-mass of the diatom and the approaching atom, and γ denotes the angle between the vector, \mathbf{R} , and the NO bond-axis, \mathbf{r} . The latter points in the same direction as the dipole moment, from the N atom to the O atom. The V_{sum} and V_{diff} CCSD(T) PESs of Alexander^{6,7} are plotted in Fig. 1. Based on the above considerations regarding Hund's case (a) behavior,⁵ one might anticipate that SO conserving collisions of NO(X) with Ar will be primarily sensitive to the V_{sum} interaction potential, whilst SO changing collisions will be particularly sensitive to V_{diff} .

Whilst there have been a large number of studies investigating the SO conserving transitions of the inelastic scattering of NO(X) with the rare gases,^{6,8–14} far less work has been devoted to SO changing transitions.^{15–18} This is due to the experimental challenges of recording SO changing transitions, which have integral cross sections which are typically around a factor of five smaller than those on the SO conserving manifold. It is therefore not surprising that until now the effects of initial bond-axis orientation on SO changing collisions have been restricted to measurement of the integral steric asymmetry.^{19–22}

The integral steric effect for NO(X) + Ar has been studied in great detail in pioneering work by Stolte and coworkers.^{17,20,22–27} Oscillations in the integral steric effect with change in rotational quantum state of the NO, Δj , have been shown to originate from quantum interference from scattering at the two ends of the molecule,^{20,22,28–30} due to the near homonuclearity of the NO(X) molecule. Whilst steric effects have been observed in both reactive and inelastic scattering,^{31–33} quantum interference mechanisms, arising from interference between scattering from either end of the molecule, are less common, and, for example, have not been observed in the bond-axis orientation resolved scattering of OH(X) radicals.^{21,34–36} In contrast to studies of the integral steric effect, very little attention has been paid to the differential steric effect in NO(X) collisions due to the greater difficulty of these experiments. However, recent work by some of the current authors, employing hexapole state selection and static field orientation techniques with velocity-map³⁷ ion imaging³⁸ (VMI) methods, successfully determined the differential steric asymmetry for spin-orbit conserving transitions of NO(X) + Ar.^{29,30} In the present investigation, we extend this study to the measurement of the differential steric effect for spin-orbit changing collisions of NO(X) with Ar.

The paper is laid out as follows. A brief theoretical description of the bond orientation resolved scattering of NO(X) with an atom is given in Section II. Methods for the experiment, data analysis, and quantum mechanical (QM) scattering calculations are then discussed in

Section III. The results of the experimental bond-axis orientation study of the SO changing transitions of NO(X) + Ar are presented in Section IV, including the ion images, bond-axis oriented DCSs, and orientation moments. Section V presents a detailed comparison of bond-axis oriented scattering for the $\Delta\Omega = 0$ and $\Delta\Omega = +1$ transitions. Finally, this is followed by conclusions in Section VI.

II. THEORY

Quantum mechanically, the field dependent state-to-state DCS, $d\sigma/d\omega \equiv d\sigma$, is proportional to the square modulus of the scattering amplitude^{6,20}

$$d\sigma_{\text{N,O}}(\theta) = \frac{1}{k^2} \sum_{m, m'} |f_{j'm'\Omega'\epsilon' \leftarrow jm\Omega E}(\theta)|^2, \quad (3)$$

where m and m' are the projections of the initial and final NO rotational angular momenta, j and j' , onto the initial relative velocity, \mathbf{k} (defined here as $\mathbf{k} = \mathbf{v}_{\text{Ar}} - \mathbf{v}_{\text{NO}}$), which is taken as the z -axis in the \mathbf{k} - \mathbf{k}' scattering frame (with $\mathbf{k}' = \mathbf{v}'_{\text{Ar}} - \mathbf{v}'_{\text{NO}}$). In what follows we will assume that the direction of the orienting static electric field, \mathbf{E} , is either parallel or antiparallel to \mathbf{k} , and hence m is also the projection along the field. Under these conditions, the scattering amplitude for NO(X) in the presence of \mathbf{E} , is given by^{6,20}

$$f_{j'm'\Omega'\epsilon' \leftarrow jm\Omega E}(\theta) = \frac{1}{\sqrt{2}} \left[|\alpha| f_{j'm'\Omega'\epsilon' \leftarrow jm\Omega e}(\theta) \pm |\beta| f_{j'm'\Omega'\epsilon' \leftarrow jm\Omega f}(\theta) \right], \quad (4)$$

where, as noted in Section I, the subscripts e/f (corresponding to spectroscopic index $\epsilon = \pm 1$) label the Λ -doublet levels, with parity $p = \epsilon(-1)^{j-1/2}$, $f_{j'm'\Omega'\epsilon' \leftarrow jm\Omega E}(\theta)$, $f_{j'm'\Omega'\epsilon' \leftarrow jm\Omega \epsilon}(\theta)$ are the scattering amplitudes for a specific state-to-state transition at a scattering angle θ for the oriented and field-free (unoriented) cases, respectively, and α and β are the field-dependent mixing parameters,

$$|\alpha(E)| = \sqrt{1 - \frac{1}{\sqrt{1 + E_{\text{red}}^2}}}, \quad |\beta(E)| = \sqrt{1 + \frac{1}{\sqrt{1 + E_{\text{red}}^2}}}. \quad (5)$$

The reduced field, E_{red} , is given by the relative strength of the orienting Stark field, W_{Stark} , and the Λ -doublet splitting, E_{Λ} :

$$E_{\text{red}} = \frac{2W_{\text{Stark}}}{E_{\Lambda}}. \quad (6)$$

In the limit of an infinite orienting field $|\alpha| = |\beta| = 1$. In the present work, the experimental field is 9.2 kV cm^{-1} and is characterized by $|\alpha| = 0.64$ and $|\beta| = 1.26$.

Combining Eqs. (3) and (4), leads to

$$\begin{aligned} d\sigma_{N,O}(\theta) = d\sigma^{-z/+z}(\theta) = \frac{1}{2k^2} \sum_{m'} \alpha^2 |f_{j'm'\Omega'\epsilon' \leftarrow jm\Omega_e}(\theta)|^2 + \beta^2 |f_{j'm'\Omega'\epsilon' \leftarrow jm\Omega_f}(\theta)|^2 \\ \pm 2|\alpha\beta| [f_{j'm'\Omega'\epsilon' \leftarrow jm\Omega_e}(\theta) f_{j'm'\Omega'\epsilon' \leftarrow jm\Omega_f}^*(\theta) + c.c.] , \quad (7) \end{aligned}$$

where *c.c.* is the complex conjugate of the last term, and $d\sigma_{N,O} \equiv d\sigma_{N,O}/d\omega$ are the oriented DCSs for collisions at the N- (\mathbf{E} along the scattering frame $-z$ axis) and O- (\mathbf{E} along the $+z$ axis) ends of the molecule, respectively.

The bond-axis oriented DCS (for scattering at the ends of the NO molecule) can also be recast in terms of the *r*-polarization dependent differential cross sections (*r*-PDDCSs), $R_q^{(k)}(\theta)$, according to^{22,29,30}

$$\begin{aligned} [d\sigma(\theta)]_{\theta_E=0,\pi} &= \frac{\sigma_{\text{iso}}}{2\pi} \left\{ R_0^{(0)}(\theta) - |\alpha\beta| R_0^{(1)}(\theta) P_1(\cos \theta_E) \right\} \\ &= \frac{\sigma_{\text{iso}}}{2\pi} \left\{ R_0^{(0)}(\theta) \mp |\alpha\beta| R_0^{(1)}(\theta) \right\} , \quad (8) \end{aligned}$$

where θ_E defines the direction of the electric field, \mathbf{E} , with respect to \mathbf{k} : as noted above, the field is parallel or anti-parallel to \mathbf{k} when $\theta_E = 0$ or $\theta_E = \pi$, corresponding to an O- ($+z$) or N- ($-z$) end collision, respectively. Comparing Eqs. (7) and (8), the specific expressions of orientation moments in terms of the scattering amplitudes can be ascertained:

$$\frac{\sigma_{\text{iso}}}{2\pi} R_0^{(0)}(\theta) = \frac{1}{2k^2} \sum_{m'} [\alpha^2 |f_{j'm'\Omega'\epsilon' \leftarrow jm\Omega_e}(\theta)|^2 + \beta^2 |f_{j'm'\Omega'\epsilon' \leftarrow jm\Omega_f}(\theta)|^2] \quad (9)$$

$$\frac{\sigma_{\text{iso}}}{2\pi} R_0^{(1)}(\theta) = \frac{1}{2k^2} \sum_{m'} [f_{j'm'\Omega'\epsilon' \leftarrow jm\Omega_e}(\theta) f_{j'm'\Omega'\epsilon' \leftarrow jm\Omega_f}^*(\theta) + c.c.] , \quad (10)$$

where σ_{iso} is the integral cross section (ICS) for isotropic (unoriented) scattering: $\sigma_{\text{iso}}/2\pi = 1/2(\sigma_O + \sigma_N)$.

The monopole term, given by

$$R_0^{(0)}(\theta) = \frac{2\pi}{\sigma_{\text{iso}}} \frac{1}{2} [d\sigma_N(\theta) + d\sigma_O(\theta)] = \frac{2\pi}{\sigma_{\text{iso}}} d\sigma_{\text{iso}}(\theta) , \quad (11)$$

is proportional to the *isotropic* DCS, $d\sigma_{\text{iso}}(\theta)$, in the presence of the orienting field, which can be written

$$\begin{aligned} d\sigma_{\text{iso}}(\theta) &= \frac{\sigma_{\text{iso}}}{2\pi} R_0^{(0)}(\theta) = \frac{1}{2} [d\sigma_N(\theta) + d\sigma_O(\theta)] \\ &= \frac{1}{2} [\alpha^2 d\sigma(\theta; j, \Omega, e \rightarrow j', \Omega', \epsilon') + \beta^2 d\sigma(\theta; j, \Omega, f \rightarrow j', \Omega', \epsilon')] . \quad (12) \end{aligned}$$

That is, the DCS $d\sigma_{\text{iso}}(\theta)$ assumes an ‘isotropic’ (field dependent) bond-axis distribution equivalent to the half-sum of the DCSs for collisions with the N- and O-ends of the molecule, or, equivalently, to the half sum of the DCSs from e and f states weighted with the field parameters.^{22,29,30} It is not the same quantity as the DCS in the absence of an orienting field, which for the selected field free $j = 1/2$ and f state would be:

$$\begin{aligned} d\sigma(\theta; 1/2, \Omega, f \rightarrow j', \Omega', \epsilon') &= \frac{1}{2k^2} \sum_{m, m'} |f_{j' m' \Omega' \epsilon' \leftarrow \frac{1}{2} m \Omega f}(\theta)|^2 \\ &= \frac{1}{k^2} \sum_{m'} |f_{j' m' \Omega' \epsilon' \leftarrow \frac{1}{2} \Omega f}(\theta)|^2. \end{aligned} \quad (13)$$

The latter would correspond to the state with $\alpha=0$ and $\beta = \sqrt{2}$.

The bond-axis orientation moments in Eqs. (9) and (10) may be related to the normalized difference differential cross section, calculated by Brouard *et al.*^{29,30}

$$d\sigma_{\text{diff}}(\theta) = \frac{d\sigma_{\text{N}}(\theta) - d\sigma_{\text{O}}(\theta)}{d\sigma_{\text{N}}(\theta) + d\sigma_{\text{O}}(\theta)} = |\alpha\beta| \frac{R_0^{(1)}(\theta)}{R_0^{(0)}(\theta)}, \quad (14)$$

where $R_0^{(1)}(\theta)/R_0^{(0)}(\theta)$ is the renormalized r -PDDCS of rank 1 and order 0. A value of this renormalized r -PDDCS greater than zero implies a preference for collisions with the N-end of the molecule, whilst a value less than zero implies a preference for scattering at the O-end of the molecule. The fact that the normalized difference differential cross section, $d\sigma_{\text{diff}}(\theta)$, must be bounded by ± 1 , implies that the renormalized r -PDDCS cannot exceed the field strength dependent limits $1/|\alpha\beta|$. This constrains the renormalized r -PDDCS to lie within ± 1.24 and ± 1.00 at the experimental (9.2 kV cm^{-1}) and infinite fields, respectively.

III. METHODS

A. Experimental methods

The crossed molecular beam apparatus used here for the differential steric effect measurements has been described in detail elsewhere,^{9,10,14,18,22,29,30} and will only be briefly discussed here. In this work, a crossed molecular beam apparatus with initial hexapole quantum state selection is coupled with final state detection *via* $(1+1')$ resonantly enhanced multi-photon ionization (REMPI) and VMI.^{37,38} The primary molecular beam is composed of 10% NO seeded in Ar, formed using a (General) valve pulsed at 10 Hz. After undergoing supersonic

expansion into vacuum, the beam is skimmed ($d = 5$ mm) and enters a hexapole, which uses the Stark effect to select the low field seeking ($\epsilon = -1$, f) Λ -doublet level of the NO(X) molecules in the beam. The secondary molecular beam is composed of pure Ar, formed *via* a pulsed (General or Jordan) valve at 5 Hz, which is skimmed ($d = 3$ mm) before it enters the scattering chamber. Background subtraction of the acquired ion image data is performed on a shot-by-shot basis. To compensate for the lower cross sections for spin-orbit changing collisions, among other measures the ion images for each final rotational state were acquired for around 200,000 laser shots to accumulate data of sufficient quality for fitting.

The orientation of the NO bond-axis before the scattering event is achieved by exposing the molecules to a static electric field (9.2 kV cm^{-1}) *via* a four-rod electrode assembly perpendicular to the initial relative velocity, \mathbf{k} .^{29,30} The NO bond-axis, \mathbf{r} , is oriented parallel or antiparallel to \mathbf{k} depending on the direction of the field, giving rise to N- or O-end collisions with the Ar collision partner. The field direction, \mathbf{E} , is switched every 1000 laser shots to record collisions at both ends of the NO molecule. (1+1') REMPI was used to state selectively ionize the scattered NO molecules by employing a probe laser tuned to the individual rotational lines of the NO(A \leftarrow X) transition (at around 226 nm), followed by ionization using 308 nm radiation from a XeCl excimer laser. VMI was used to extract ions onto a two-dimensional imaging detector. To allow velocity mapping, all four rods of the orientation electrodes were switched to a voltage of ~ 1 kV approximately 500 ns before the laser was fired, as described in detail elsewhere.^{29,30}

Two sets of data are presented in this work, in which a difference in collision energy arises from the type of valve used to create the secondary molecular beam: the Jordan and General valves, which yielded mean collision energies of 651 cm^{-1} and 532 cm^{-1} , respectively. Only the e final Λ -doublet states were recorded, as at the experimental field strength the final Λ -doublets are approximately equivalent. All data were recorded on the overlapping $Q_{21} + R_{11}$ branches, using unpolarized light, except for the $|j' = 4.5, \Omega' = 1.5, \epsilon' = e\rangle$ state, which was recorded on the P_{12} branch because the mixed branch overlaps the R_{22} branch for the $|j' = 1.5, \Omega' = 1.5, \epsilon' = f\rangle$ state.

B. Data Analysis

The raw experimental ion image is composed of a distorted ‘crushed’ Newton sphere with a marked asymmetry about the relative velocity vector, \mathbf{k} . This asymmetry arises from the laboratory (lab) to center-of-mass (CM) transformation, and the convolution of the CM frame angular distributions with several detection efficiency factors, including the flux-density correction, which must be accounted for by the analysis process. The analysis method used here for data fitting has been described in detail previously,^{9,10,18} and requires no modifications for the initial bond orientation in the current experiment. A Monte Carlo method⁹ is used to generate a set of basis images (accounting for the variation in detection probability due to experimental geometry and laser polarization parameters), which are then weighted and summed to fit the experimental image. The coefficients for each basis function are then used to calculate a DCS according to the weighted sum of Legendre polynomials. Whilst the relative difference in intensity between the two DCSs is known (from the integral steric asymmetry, see Eq. (15)), the absolute cross section for the collision is not measured. Consequently, it is necessary to normalize both DCSs (using the same factor so as to retain the integral steric effect) to the QM DCSs to facilitate comparison.

C. Quantum mechanical scattering calculations

The experimental data were compared to the results of full close-coupled (CC) QM scattering calculations carried out on the V_{sum} and V_{diff} potentials of the NO + Ar CCSD(T) PESs of Alexander,^{6,7} using the HIBRIDON suite of codes.³⁹ The NO bond length was fixed in these calculations at its equilibrium distance. Calculations were performed at the two mean experimental collision energies, $E_{\text{coll}} = 532 \text{ cm}^{-1}$ and $E_{\text{coll}} = 651 \text{ cm}^{-1}$. To account for the spread of collision energies, DCSs were calculated over a range of collision energies between 500–560 cm^{-1} with a spacing of 15 cm^{-1} , and 530–740 cm^{-1} with a spacing of 30 cm^{-1} for the mean collision energies of 532 cm^{-1} and 651 cm^{-1} , respectively. The calculated DCSs were then weighted with Gaussian distributions with a FWHM of 35 cm^{-1} to simulate the experimental results. Rotational levels up to $j' = 20.5$, both Λ -doublet levels ($\epsilon = \pm 1$) and SO manifolds ($\Omega = 0.5, 1.5$) were included in the scattering wave function. The maximum partial wave was set to $J = 180.5$ to achieve convergence of the calculation. As already

indicated, in these calculations it was assumed that the electric field, \mathbf{E} , in the interaction region is oriented either parallel or antiparallel to the initial relative velocity, \mathbf{k} . Collisions for which the bond-axis, \mathbf{r} , is parallel (antiparallel) to \mathbf{k} are N-end (O-end). The former are induced when $\theta_E = 180^\circ$, while the latter correspond to $\theta_E = 0^\circ$. The PESs are defined such that $\gamma = 0^\circ$ corresponds to an O-end collision (Ar–ON). Finally, the experimental observables were calculated using Eqs. (3) to (14).

It is perhaps worth noting that whilst quasi-classical trajectory calculations have been undertaken previously to model the SO conserving transitions, using the V_{sum} PES,^{9,29,30,40} no attempt has been made here to model the SO changing collisions of NO(X) + Ar using classical methods.

IV. RESULTS

A. Ion images

Figs. 2 and 3 show the experimental and fitted ion images for the bond-axis orientation resolved SO changing transitions $|j = 0.5, \Omega = 0.5, E\rangle \rightarrow |j', \Omega' = 1.5, e\rangle$ at $E_{\text{coll}} = 651 \text{ cm}^{-1}$ and 532 cm^{-1} , respectively. Note that the images in the two figures were recorded using slightly different VMI voltages. The initial relative velocity vector, \mathbf{k} , is superimposed onto the top left experimental image shown in Fig. 2. For each final rotational state, the colour scale (where red is the maximum intensity) is the same for N- and O-end collisions so as to preserve the relative intensity differences observed between the two bond-axis orientations (see further below). The agreement between the experimental images and the fits to the data is generally good, with all experimentally resolved features being reasonably well captured by the fits.

Many of the general trends observed in the ion images can be explained using similar arguments to those employed in absence of orienting static field, when the initial Λ -doublet level (f) is unmixed.^{9,16,18} As discussed in Section III B, there is a marked asymmetry about the relative velocity vector, \mathbf{k} , in each image, due to flux-density effects, which is generally well-accounted for in the fitted images. As the final rotational state, j' , increases the radius of the ion images becomes smaller as a greater proportion of the initial translational energy of the system is converted into rotational energy, and the outgoing velocity is thereby

reduced. The distribution of intensity in the ion images also changes with increasing j' : for low rotational excitation, intensity is predominantly forward and sideways scattered, whereas for high rotational excitation the ion images become more sideways and backward scattered. This can be rationalized by considering the types of collision that give rise to different amounts of rotational energy transfer (RET). Only small amounts of energy can be transferred in glancing-type (larger impact parameter) collisions, which give rise to forward scattering, whilst much larger RET (leading to rotational excitation to higher j' levels) is achieved for head-on collisions, which are more direct, and typically give rise to backwards scattering.

The orientation-dependent ion images for the SO changing ($\Delta\Omega = +1$) collisions, shown in Figs. 2 and 3, also display many of the general features observed for the SO conserving ($\Delta\Omega = 0$) transitions.^{29,30} However, unlike for the $\Delta\Omega = 0$ transitions,^{29,30} in which scattering is confined to the forward region for low Δj , for the $\Delta\Omega = +1$ transitions intensity is observed over a wide range of scattering angles for all final rotational states. This arises because SO changing collisions tend to occur at smaller impact parameters (involving more head-on collisions) and, consequently, scattering appears also in the backward hemisphere, even for low Δj transitions, for reasons discussed in detail in Section V.

Differences between scattering from the two initial orientations of the NO bond axis are clearly observed in the experimental and fitted images. In general, the ion images show that the scattered signal due to collisions with the N-end of the NO molecule are more intense, compared to scattering from the O-end of the molecule. This is consistent with the integral steric asymmetry^{20,29,30} shown in Fig. 4 (reproduced here for convenience from Ref. 22), and defined as

$$S_z = \frac{\sigma_N - \sigma_O}{\sigma_N + \sigma_O}, \quad (15)$$

where $\sigma_{N,O}$ are the integral cross sections for scattering from the N- and O-ends of the NO molecule, obtained by integration of $d\sigma_{N,O}$, Eq. (3), over the scattering and the azimuthal angles. (The right panel of Fig. 4 includes the integral steric asymmetry calculated using only the V_{sum} or the $V_{00} + V_{\text{diff}}$ potentials, and is discussed further in Section V.) While oscillations in S_z are observed for different final rotational states, due to quantum interference between scattering from both orientations of the molecule,^{20,22} there is an overall preference for $S_z > 0$, corresponding to more intense scattering off the N-end of the molecule ($\sigma_N > \sigma_O$). States with a negative value of S_z correspond to more intense scattering off the O-end of the

molecule, which is observed as increased intensity in the O-end ion images relative to those for the N-end; this is particularly obvious for $j' = 8.5$ and $j' = 10.5$. Whilst similar features are observed in the ion images for collisions with the N- and O-ends of the molecule, the relative intensities of the features observed in the two images is clearly seen to differ due to the effects of the integral steric asymmetry.

The raw ion images shown in Figs. 2 and 3 clearly display the same intensity alternations with Δj between the N- and O-end collisions as observed in the integral steric asymmetry shown in Fig. 4. More detailed inspection of the image data in Figs. 2 and 3 further reveals that the location of the peaks in intensity of the ion images tends to be similar for the two bond-axis orientations, whilst the relative intensities of these features often varies between the two geometries. This feature of the ion images has been noted previously for the $\Delta\Omega = 0$ collisions, and is also observed in the experimentally derived and QM calculated DCSs presented below in Section IV B.

B. Bond-axis oriented DCSs

The experimentally determined bond orientation resolved DCSs, $d\sigma_{\text{N,O}}$, are shown in Figs. 5 and 6 alongside the corresponding QM calculated DCSs. The figure also includes the ‘isotropic’ DCSs in the presence of a field, see Eq. (12), which are displayed as the grey shaded areas. The QM calculated and experimentally determined DCSs at the two collision energies are quite similar (*cf.* the DCSs shown in Figs. 5 and 6), with very slightly more forward scattering observed on average at the higher collision energy.

The agreement between the QM and experimental DCSs is generally acceptable, with the higher collision energy data being in slightly better agreement than those obtained at the lower energy, where the ion images are slightly more distorted in appearance due to the switching of the static field. Some of the theoretical DCSs for low Δj , particularly $\Delta j = 3$ to 6, exhibit a sharp peak and rapid oscillations confined to the forward direction¹² which is not well reproduced by the current experiments. This is due to the limited angular resolution of the instrument employed, which is around 20° . Similar observations have been made in previous studies^{9,40}. The agreement between experiment and theory for $j' = 7.5$ is noticeably worse than for the other final states. This may reflect errors in the QM theoretical DCSs, but we believe it is more likely that the discrepancy in this case can be explained

by the position of the scattered intensity in the experimental ion image. For this particular rotational state, the scattered NO molecules have final CM velocities which coincide with the position of the lab frame origin (corresponding to zero speed in the LAB frame). This subset of NO molecules is thus nearly stationary in the lab frame and therefore remains in the laser overlap (detection) volume for a longer time. For this reason, these molecules have a higher detection efficiency than the molecules with larger lab speeds. For these slow moving molecules, any small errors in the calculations of the flux-density correction and detection efficiency factors can result in a relatively poor fit for the experimental data. This effect is also observed, although to a lesser extent, in the experimental images and DCSs for $j' = 6.5$ and 8.5 , where the main intensity in the ion image also coincides quite closely with the lab frame origin.

Some differences may be observed in the oriented DCSs between collisions at the N- and O-ends of the molecule, although due to the broadness of the peaks for these $\Delta\Omega = +1$ collisions the differences are not so clear as for the $\Delta\Omega = 0$ transitions.^{29,30} As is the case for the DCSs obtained in the absence of a static field,^{9,40} oriented DCSs for the $\Delta\Omega = +1$ transitions show more uniform scattering intensity than the $\Delta\Omega = 0$ collisions, with the peaks in the SO changing DCSs generally superimposed on top of a relatively broad background of scattering intensity. On average, scattering from the N-end of the molecule leads to somewhat more forward scattering than collisions at the O-end of the molecule, reflecting the fact that both V_{sum} and V_{diff} extend to slightly longer range at the N-end of the molecule. As already observed in the raw ion images, the angular distributions for collision at the two ends of the NO molecule generally contain the same number of peaks in the DCS, whilst the relative intensity, particularly of the two most prominent peaks, varies between the N- and O-ends. This effect is most obvious for intermediate j' (for example, between 9.5 and 11.5), for which the two peaks show a strong difference in intensity depending on which end of the molecule undergoes scattering. For $j' = 10.5$, for example, this is observed as two separate peaks in the DCS of the N-end of the molecule, whilst at the O-end of the molecule the second (larger scattering angle) peak is more intense, and appears as a shoulder on the first peak in the DCS. Similar general behavior has been observed for the SO conserving transitions.^{29,30}

As for the $\Delta\Omega = 0$ transitions,^{29,30} no evidence is observed in either the experimental ion images or the DCSs for the presence of parity pairs; states with the same $n = j' - \epsilon\epsilon'/2$

and the same total parity. In the absence of an orienting field, parity pairs^{9,18,26,41} result in similar structures observed in the DCSs of adjacent j' final states for a pair $|j' = n + 0.5, f\rangle$ and $|j' = n - 0.5, e\rangle$ from the $j = 0.5$ state of $\epsilon = -1, f$ parity (which are Λ -doublet conserving and changing, respectively, but both either conserve or change parity during collision). This effect arises since the two states are coupled by the same matrix elements in the potential, leading to similar dynamics.^{5,18,42,43} When the bond-axis is initially oriented by an electric field the two initial Λ -doublets are mixed, and thus the initial wave function no-longer has a specific initial parity. Whilst the final rotational state has a definite parity ($\epsilon = +1, e$ here), the overall transition is neither parity conserving nor parity changing due to the superposition of the initial Λ -doublet states. The dynamics of the two states are no longer coupled by exactly the same terms in the potential, and thus parity pairs are not observed in any of the recorded states.

C. r -Polarization dependent differential cross sections

The renormalized (1,0) r -PDDCS moment, $R_0^{(1)}(\theta)/R_0^{(0)}(\theta)$, which apart from the $|\alpha\beta|$ factor is equal to $d\sigma_{\text{diff}}(\theta)$ (see Eq. (14)), provides a measure of the difference in the angular scattering distribution for the two ends of the NO molecule. Figs. 7 and 8 show the experimental and QM renormalized (1,0) bond orientation moments for the $|j = 0.5, \Omega = 0.5, E\rangle \rightarrow |j', \Omega' = 1.5, \epsilon' = e\rangle$ transitions at mean collision energies of 651 cm^{-1} and 532 cm^{-1} , respectively. Typically, the experimental and QM renormalized (1,0) moments follow the same trend, although not all of the features in the QM data are reproduced experimentally, mostly due to the limited experimental resolution. In general, the agreement between experiment and theory is somewhat less good than in the case of the oriented DCSs themselves due to the additional errors associated with taking the normalized difference between the DCSs for scattering at the two ends of the molecule. However, in the case of $j' = 7.5$, the experimental renormalized (1,0) moment at the two collision energies are in a reasonable agreement with the QM data, in spite of the disagreement between the QM and experimental oriented DCSs. This is mainly due to an error cancelation: the errors in the lab frame detection efficiencies will be nearly the same for collisions at either end of the NO molecule, and by subtraction the errors are largely cancelled out.

A negative value of the renormalized (1,0) r -PDDCS moment, $R_0^{(1)}(\theta)/R_0^{(0)}(\theta)$, corre-

sponds to preferential scattering from the O-end of the molecule ($d\sigma_O > d\sigma_N$), whereas a positive value corresponds to preferential scattering off the N-end, ($d\sigma_N > d\sigma_O$). In the particular case of the $\Delta j = 10$ to 12 transitions, the experimental values of the renormalized (1,0) r -PDDCS moments approach -1.24 at small scattering angles. This arises because the angular distribution in the N-end geometry, $d\sigma_N(\theta)$, approaches zero, and, hence, the experiment indicates a strong preference for collisions with the O-end of the molecule. However, it should be noted that in the small region of forward scattering in question the errors associated with these particular renormalized (1,0) r -PDDCS moments become very large, and the results are probably not that significant at these scattering angles.

As observed clearly in the experimental ion images (and more subtly in the extracted DCSs) the general preference is for scattering from the N-end of the NO molecule, which is manifest as a positive value of the renormalized (1,0) moment. Note that integration of the unnormalized r -PDDCSs, $R_0^{(1)}(\theta)$, over scattering angle, including the $\sin \theta$ weighting, recovers the integral steric asymmetries shown in Fig. 4, which clearly show a preference for N-end collisions for the SO changing collisions. The oscillations observed in the integral steric asymmetry for adjacent Δj , shown in Fig. 4,^{22,30} are also evident in the renormalized r -PDDCS: for example, the overall preference is for the N-end of the molecule for $j' = 9.5$ and the O-end for $j' = 10.5$. The alternation of positive (N-end) and negative (O-end) steric effect is much less obvious than for the $\Delta\Omega = 0$ transitions.³⁰ The overall preference for the N-end of the molecule, which arises from the combined effects of the V_{sum} and V_{diff} potentials, is discussed further in Section V.

V. DISCUSSION

A. General observations

The bond-axis orientation data for the SO changing collisions of $\text{NO(X)} + \text{Ar}$ presented in Section IV complements similar results obtained previously for the SO conserving transitions.^{29,30} Both data sets confirm the importance of quantum interference effects in determining the scattering intensity for even and odd Δj transitions. More subtle differences in the DCSs for N- versus O-end collisions, which are primarily observed as changes in peak intensity in the DCS, rather than peak position, arise from the differences in the scattering

dynamics at the two ends of the molecule. These latter differences partly reflect the slight mass asymmetry of NO, as well as differences in the PESs at the two ends of the molecule. Collisions at the N-end of NO are generally found to lead to somewhat higher intensity in the forward scattered region, consistent with the location of the CM being slightly shifted towards the O-atom, and the somewhat stronger long-range attraction at the N-end of the molecule.

B. Effect of spin-orbit manifold

We consider here in more detail the differences in bond-axis orientation effects for SO conserving and changing collisions. It is worth noting at the outset that the complexity of the V_{diff} potential, which under pure Hund's case (a) would govern SO changing transitions, and the likely differing contributions of the V_{sum} and V_{diff} potentials to both the SO conserving and changing collisions with increasing Δj , make it difficult to provide simple explanations for the differences observed between bond-axis oriented and unoriented scattering into the two final state SO manifolds. Fig. 9 presents the calculated ICSs for N- and O-end collisions of $\text{NO}(\text{X}) + \text{Ar}$ obtained at a fixed collision energy of $E_{\text{coll}} = 651 \text{ cm}^{-1}$ and at the static electric field used in the experiments, 9.2 kV cm^{-1} , for SO conserving (left column) and SO changing collisions (right column). The ICSs were determined from calculations employing the full PESs of Alexander^{6,7} (top row), on the V_{sum} PES only (middle row), and on $V_{00} + V_{\text{diff}}$ PES only (bottom row). The total cross sections, summed over Δj , are also given in each panel. These results provide important information about the role of V_{sum} and V_{diff} . Whilst SO conserving ICSs can be approximated quite well using the V_{sum} PES alone, it is very striking that scattering on the $V_{00} + V_{\text{diff}}$ PES alone cannot account for the SO changing collisions. In the latter case, one must use the full PESs, *i.e.* both V_{sum} and V_{diff} , to obtain quantitative agreement with the exact ICS data, even at low Δj where one might expect Hund's case (a) behavior to reasonably apply. It is also noteworthy that inclusion of the V_{diff} PES plays an important role in determining the N-end preference for the ICSs in the SO changing case.

Bearing in mind these issues, Fig. 10 shows the QM $R_0^{(0)}(\theta)$ and $R_0^{(1)}(\theta)$ bond-axis orientation moments, as well as the renormalized (1,0) r -PDDCS of Eq. (14), for both SO conserving ($\Delta\Omega = 0$) and SO changing ($\Delta\Omega = +1$) collisions at a fixed collision energy of

651 cm⁻¹. The results are shown for scattering into the final e Λ -doublet levels of several final rotational states ($j' = 2.5, 7.5, 12.5$, and 15.5). As discussed in Section II, the (0,0) moment describes the ‘isotropic’ DCS, *i.e.* the DCS associated with scattering from an initial state which is a coherent superposition of the two components of the Λ -doublet weighted with the field dependent mixing parameters, α and β , according to Eq. (12).^{22,29,30} The (1,0) r -PDDCS moment describes the effect of orientation of the NO bond axis with respect to the initial relative velocity vector, \mathbf{k} .

Comparison of the (0,0) moments reveals the differences between the ‘isotropic’ DCSs for the $\Delta\Omega = 0$ and $\Delta\Omega = +1$ transitions (see the red lines in the top two rows of Fig. 10). On average, the (0,0) moment for SO changing collisions is more backward scattered than for its SO conserving counterpart, as has previously been observed in the DCSs for field free scattering.¹⁸ The more backward scattering observed for SO changing collisions reflects the fact that the latter take place on average *via* more head-on, low impact parameter (low partial wave) collisions than for SO conserving transitions. There are two reasons for this behavior. Firstly, RET collisions for $\Delta\Omega = +1$ are more endothermic processes than $\Delta\Omega = 0$ transitions, requiring an extra 123 cm⁻¹, and therefore impairing glancing collisions, which are predominantly forward scattered, to take place. The second reason lies in the difference between the V_{sum} and V_{diff} PESs, shown in Fig. 1. As can be seen, V_{diff} is mainly negative, but with a considerably shorter range than V_{sum} , such that the attractive part of the V_{sum} PES extends well beyond the V_{diff} PES. In both cases, the extent of the potentials is significantly larger at the N-end than at the O-end of the molecule. As already noted in Section I, for Hund’s case (a) molecules (which is a reasonable approximation for the low j' states of NO), SO conserving collisions take place on the V_{sum} PES, whilst SO changing collisions are controlled by V_{diff} . Therefore, for low and moderate Δj , the longer range of the V_{sum} PES relative to the V_{diff} PES results in larger impact parameter (partial wave) collisions for SO conserving transitions, which induce more forwards scattered products than the smaller impact parameters which occur for SO changing collisions. As Δj increases, the rotation of the NO molecule is best described as intermediate between Hund’s case (a) and (b), and both the sum and difference potentials become important in the resulting scattering. Therefore, the repulsive wall on the V_{sum} potential becomes important for both $\Delta\Omega = 0$ and $\Delta\Omega = +1$ collisions, leading generally to more backwards scattering. This is supported by the presence of oscillations in the integral steric asymmetry for the SO changing collisions

shown in Fig. 4, which are known to arise from interference between repulsive collisions, and further by the fact that S_z cannot be completely described by only the difference potential (see the right panel of Fig. 4).²²

The (1,0) r -PDDCS orientation moments for SO conserving and changing collisions (see the blue dashed lines in the top two rows of Fig. 10) are similar in structure for scattering into the same final j' state, although as in the case of the integral steric effect, the moments are generally somewhat more positive for $\Delta\Omega = +1$ than $\Delta\Omega = 0$ collisions, corresponding to a stronger preference for N-end collisions. The similarity in structure of the moment suggests that similar arguments may be used to understand the differential steric effect for both SO manifolds. The renormalized (1,0) r -PDDCS moments, $R_0^{(1)}(\theta)/R_0^{(0)}(\theta)$, displayed in the bottom row of Fig. 10, provide more useful information about the effect of bond-axis orientation with respect to \mathbf{k} independent of the overall scattering distribution, described by $R_0^{(0)}(\theta)$. Thus, the renormalized (1,0) moments depend only on the effects of bond-axis orientation, and allow direct comparison to be made concerning the steric effect for the $\Delta\Omega = 0$ and $\Delta\Omega = +1$ transitions. As was clear from the $R_0^{(1)}(\theta)$ moments, the renormalized (1,0) moments are generally more positive for the SO changing transitions than for the corresponding SO conserving transitions, confirming that N-end collisions are more strongly favoured for SO changing collisions than for SO conserving transitions. This is perhaps not surprising given that the V_{diff} is more anisotropic than V_{sum} , and has a more extended range at the N-end of the molecule compared with the O-end (see Fig. 1).

Whilst the renormalized (1,0) moments for the SO conserving and changing collisions are generally quite similar, for low rotational energy transfer substantial differences are observed. For example, the renormalized moment for $j' = 2.5$ shows oscillatory structure for the $\Delta\Omega = 0$ transition and is generally negative (favouring O-end collisions), whilst for $\Delta\Omega = +1$ N-end collisions are clearly favoured for all scattering angles. This is understandable since features whose origin lies in the long-range attractive part of the PES, such as glory scattering and ℓ -type rainbows, are known to be observed for transitions within the SO conserving manifold, but are less important (or non-existent) for SO changing transitions, due to the shorter range of the difference potential.^{18,40}

VI. CONCLUSIONS

In this article, the end-on bond-axis orientation resolved differential cross sections for SO changing transitions of NO with Ar are presented, and compared with the results from QM scattering calculations. In the experiments, a static electric field, \mathbf{E} , is oriented either parallel or antiparallel to the initial relative velocity, \mathbf{k} . The measured DCSs show significant differences between collisions of Ar with the N- and O-end of the NO molecule. The experimentally derived DCSs were generally found to be in reasonable agreement with the results from QM scattering calculations. For both ends of the NO molecule, the general structure of the DCSs was found to be similar to those observed for unoriented collisions in the absence of a static electric field.⁹ As with the bond-axis oriented DCSs for the SO conserving collisions,^{29,30} parity pair behavior^{9,18,26,41} was not observed, as a consequence of the mixing of the initial Λ -doublet states by the orienting field. The observed overall preference for collisions at the N-end of the molecule can be related to differences in the topographies of the N- and O-end regions of both V_{sum} and V_{diff} PESs. The bond-axis oriented scattering for the SO changing transitions was shown to be quite similar to that observed for SO conserving collisions, although the (1,0) renormalized r -PDDCSs were generally more positive for $\Delta\Omega = +1$ SO changing collisions, reflecting a stronger preference for N-end collisions than for $\Delta\Omega = 0$ SO conserving collisions.

ACKNOWLEDGMENTS

The support of the UK EPSRC (to M.B. *via* Programme Grant EP/L005913/1). S.S. acknowledges support from the National Basic Research Program of China (973 program) under grant No. 2013CB922200, and from the National Science Foundation of China under grant Nos. 11034003 and 91221301. F.J.A. acknowledges the support of the Spanish Ministry of Economy and Innovation (Grant CTQ2015-65033-P MINECO-FEDER). S.D.S.G. and M.B. also thank Cambio Ltd. and Dr Peter Dean for generous support, and Dr Cornelia Heid for critically reading the manuscript.

REFERENCES

- ¹D. H. Parker and R. B. Bernstein, *Ann. Rev. Phys. Chem.*, 1989, **40**, 561–595.

- ²H. J. Loesch, *Ann. Rev. Phys. Chem.*, 1995, **46**, 555–594.
- ³F. J. Aoiz, M. Brouard, S. D. S. Gordon, B. Nichols, S. Stolte and V. Walpole, *Phys. Chem. Chem. Phys.*, 2015, **17**, 30210–30228.
- ⁴C. Amiot, *J. Mol. Spectrosc.*, 1982, **94**, 150–172.
- ⁵M. H. Alexander, *J. Chem. Phys.*, 1982, **76**, 5974–5988.
- ⁶M. H. Alexander, *J. Chem. Phys.*, 1993, **99**, 7725–7738.
- ⁷M. H. Alexander, *J. Chem. Phys.*, 1999, **111**, 7435–7439.
- ⁸M. Yang and M. H. Alexander, *J. Chem. Phys.*, 1995, **103**, 6973–6983.
- ⁹C. J. Eyles, M. Brouard, C.-H. Yang, J. Klos, F. J. Aoiz, A. Gijsbertsen, A. E. Wiskerke and S. Stolte, *Nat. Chem.*, 2011, **3**, 597–602.
- ¹⁰M. Brouard, H. Chadwick, C. J. Eyles, B. Hornung, B. Nichols, J. M. Scott, F. J. Aoiz, J. Klos, S. Stolte and X. Zhang, *Mol. Phys.*, 2013, **111**, 1759–1771.
- ¹¹M. Brouard, H. Chadwick, C. J. Eyles, B. Hornung, B. Nichols, F. J. Aoiz, P. G. Jambrina and S. Stolte, *J. Chem. Phys.*, 2013, **138**, 104310.
- ¹²A. von Zastrow, J. Onvlee, S. N. Vogels, G. C. Groenenboom, A. van der Avoird and S. Y. T. van de Meerakker, *Nat. Chem.*, 2014, **6**, 216–221.
- ¹³H. Chadwick, B. Nichols, S. D. S. Gordon, B. Hornung, E. Squires, M. Brouard, J. Klos, M. H. Alexander, F. J. Aoiz and S. Stolte, *J. Phys. Chem. Lett.*, 2014, **5**, 3296–3301.
- ¹⁴M. Brouard, H. Chadwick, S. D. S. Gordon, B. Hornung, B. Nichols, J. Klos, F. J. Aoiz and S. Stolte, *J. Chem. Phys.*, 2014, **141**, 164306.
- ¹⁵H. Kohguchi, T. Suzuki and M. H. Alexander, *Science*, 2001, **294**, 832–834.
- ¹⁶M. S. Eliooff and D. W. Chandler, *J. Chem. Phys.*, 2002, **117**, 6455–6462.
- ¹⁷M. J. L. de Lange, S. Stolte, C. A. Taatjes, J. Klos, G. C. Groenenboom and A. van der Avoird, *J. Chem. Phys.*, 2004, **121**, 11691–11701.
- ¹⁸C. J. Eyles, M. Brouard, H. Chadwick, F. J. Aoiz, J. Klos, A. Gijsbertsen, X. Zhang and S. Stolte, *Phys. Chem. Chem. Phys.*, 2012, **14**, 5420–5439.
- ¹⁹M. H. Alexander, *Faraday Discuss.*, 1999, **113**, 437–454.
- ²⁰M. H. Alexander and S. Stolte, *J. Chem. Phys.*, 2000, **112**, 8017–8026.
- ²¹M. C. van Beek, J. J. ter Meulen and M. H. Alexander, *J. Chem. Phys.*, 2000, **113**, 637–646.
- ²²M. Brouard, S. D. S. Gordon, A. Hackett Boyle, C. G. Heid, B. Nichols, V. Walpole, F. J. Aoiz and S. Stolte, *J. Chem. Phys.*, 2017, **146**, 014302.

- ²³J. van Leuken, J. Bulthuis, S. Stolte and J. Snijders, *Chem. Phys. Lett.*, 1996, **260**, 595–603.
- ²⁴M. de Lange, M. Drabbels, P. Griffiths, J. Bulthuis, S. Stolte and J. Snijders, *Chem. Phys. Lett.*, 1999, **313**, 491–498.
- ²⁵A. Gijsbertsen, H. Linnartz, J. Kłos and S. Stolte, *Phys. Scr.*, 2005, **72**, C1–C5.
- ²⁶A. Gijsbertsen, H. Linnartz, C. A. Taatjes and S. Stolte, *J. Am. Chem. Soc.*, 2006, **128**, 8777–8789.
- ²⁷C. A. Taatjes, A. Gijsbertsen, M. J. L. de Lange and S. Stolte, *J. Phys. Chem. A*, 2007, **111**, 7631–7639.
- ²⁸A. Ballast, A. Gijsbertsen, H. Linnartz and S. Stolte, *Mol. Phys.*, 2008, **106**, 315–331.
- ²⁹B. Nichols, H. Chadwick, S. D. S. Gordon, C. J. Eyles, B. Hornung, M. Brouard, M. H. Alexander, F. J. Aoiz, A. Gijsbertsen and S. Stolte, *Chem. Sci.*, 2015, **6**, 2202–2210.
- ³⁰M. Brouard, H. Chadwick, S. D. S. Gordon, B. Hornung, B. Nichols, F. J. Aoiz and S. Stolte, *J. Chem. Phys.*, 2016, **144**, 224301.
- ³¹H. J. Loesch and J. Møller, *J. Chem. Phys.*, 1992, **97**, 9016–9030.
- ³²H. J. Loesch and F. Stienkemeier, *J. Chem. Phys.*, 1994, **100**, 4308–4315.
- ³³H. Ohoyama and Y. Matsuura, *J. Phys. Chem. A*, 2011, **115**, 8055–8063.
- ³⁴M. C. Van Beek, G. Berden, H. L. Bethlem and J. J. Ter Meulen, *Phys. Rev. Lett.*, 2001, **86**, 4001–4004.
- ³⁵M. C. van Beek and J. J. ter Meulen, *J. Chem. Phys.*, 2001, **115**, 1843–1852.
- ³⁶R. Cireasa, A. Moise and J. J. ter Meulen, *J. Chem. Phys.*, 2005, **123**, 064310.
- ³⁷A. T. J. B. Eppink and D. H. Parker, *Rev. Sci. Instrum.*, 1997, **68**, 3477–3484.
- ³⁸D. W. Chandler and P. L. Houston, *J. Chem. Phys.*, 1987, **87**, 1445–1447.
- ³⁹HIBRIDON is a package of programs for the time-independent quantum treatment of inelastic collisions and photodissociation written by M. H. Alexander, D. E. Manolopoulos, H.-J. Werner and B. Follmeg, with contributions by P. F. Vohralik, D. Lemoine, G. Corey, R. Gordon, B. Johnson, T. Orlikowski, A. Berning, A. D. Esposti, C. Rist, P. Dagdigian, B. Pouilly, G. van der Sanden, M. Yang, F. de Weerd, S. Gregurick and J. Kłos.
- ⁴⁰C. J. Eyles, M. Brouard, H. Chadwick, B. Hornung, B. Nichols, C.-H. Yang, J. Kłos, F. J. Aoiz, A. Gijsbertsen, A. E. Wiskerke and S. Stolte, *Phys. Chem. Chem. Phys.*, 2012, **14**, 5403–5419.

- ⁴¹A. Gijsbertsen, H. Linnartz, G. Rus, A. E. Wiskerke, S. Stolte, D. W. Chandler and J. Kłos, *J. Chem. Phys.*, 2005, **123**, 224305.
- ⁴²J. Kłos, F. J. Aoiz, J. E. Verdasco, M. Brouard, S. Marinakis and S. Stolte, *J. Chem. Phys.*, 2007, **127**, 031102.
- ⁴³F. J. Aoiz, J. E. Verdasco, M. Brouard, J. Kłos, S. Marinakis and S. Stolte, *J. Phys. Chem. A*, 2009, **113**, 14636–14649.

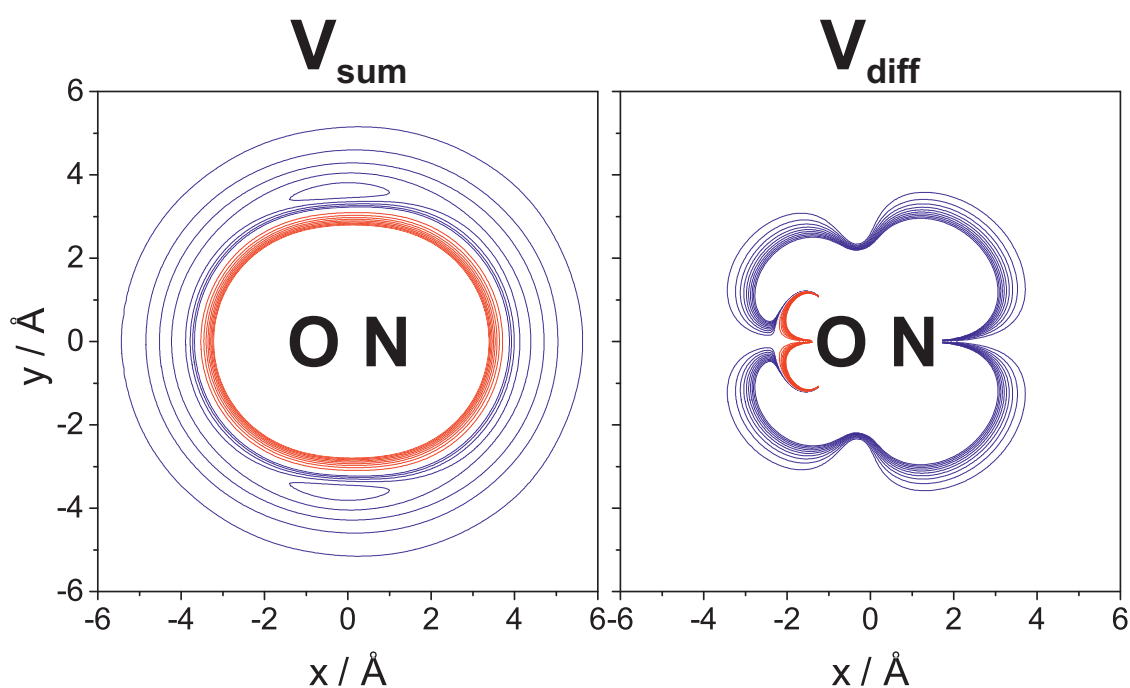


FIG. 1. V_{sum} (left) and V_{diff} (right) potential energy surfaces for the NO(X) + Ar system.^{6,7} The attractive (blue) and repulsive (red) contours are separated by 20 cm^{-1} and 100 cm^{-1} , respectively.

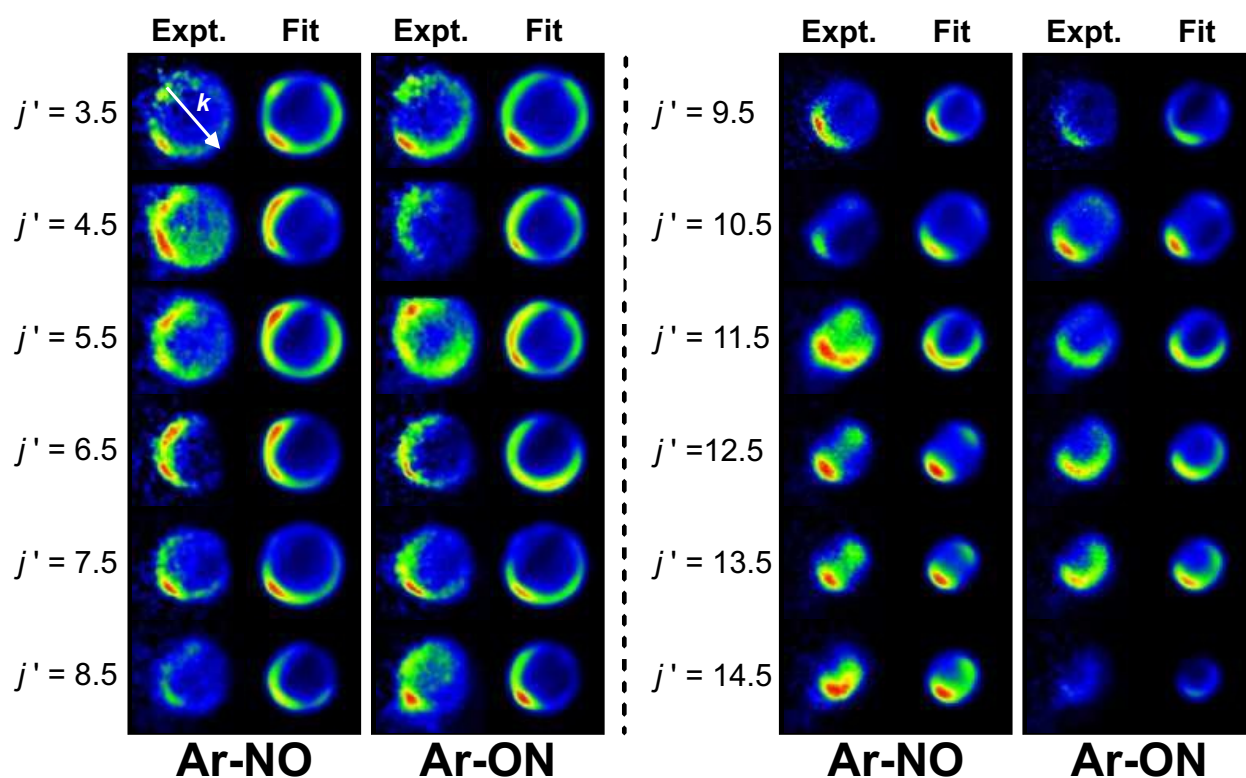


FIG. 2. Experimental (left) and fitted (right) ion images for the bond-orientation resolved spin-orbit changing collisions of NO with Ar, at a mean collision energy $E_{\text{coll}} = 651 \text{ cm}^{-1}$ and at the static electric field used in the experiments, 9.2 kV cm^{-1} , into final rotational states defined by $|j' \Omega' = 1.5, \epsilon' = e\rangle$. The N-end ($-z$) and O-end ($+z$) collisions are shown in columns 1 and 3, and 2 and 4, respectively. The white arrow in the top left hand panel indicates the direction of the initial relative velocity, \mathbf{k} .

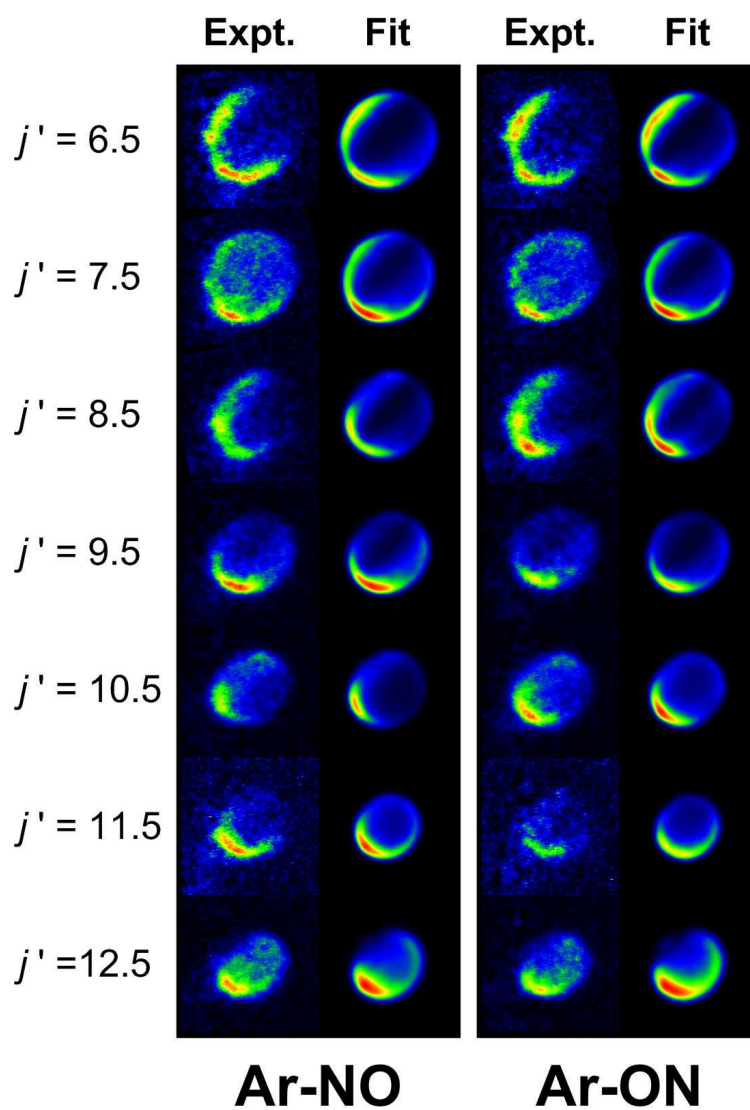


FIG. 3. Same as Fig. 2, but at a mean collision energy $E_{\text{coll}} = 532 \text{ cm}^{-1}$.

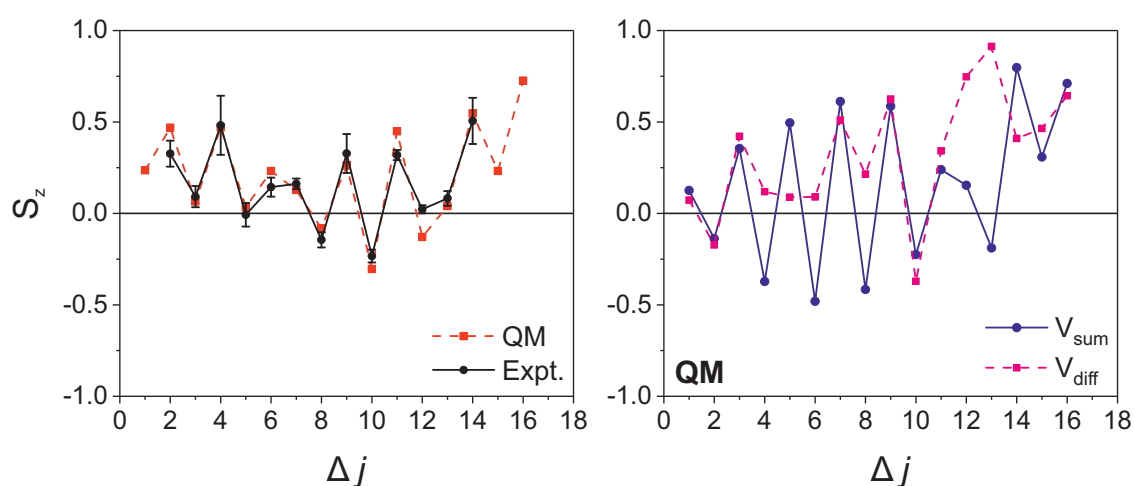


FIG. 4. Left: Comparison of the experimental (black line with circles) and QM (red dashed line with squares) integral steric asymmetry for NO(X) + Ar scattering, at $E_{\text{coll}} = 651 \text{ cm}^{-1}$ and at the static electric field used in the experiments, 9.2 kV cm^{-1} , on the spin-orbit changing manifold, with $\epsilon' = e$. Right: As in the left panel but showing the integral steric asymmetry calculated using only the V_{sum} (blue circles with continuous line) or the $V_{00} + V_{\text{diff}}$ (red squares with dashed line) potentials. Adapted from Brouard *et al.* Ref. 22. (Note that the labelling shown here in the right panel was incorrectly inverted in Fig. 2 of Ref. 22.)

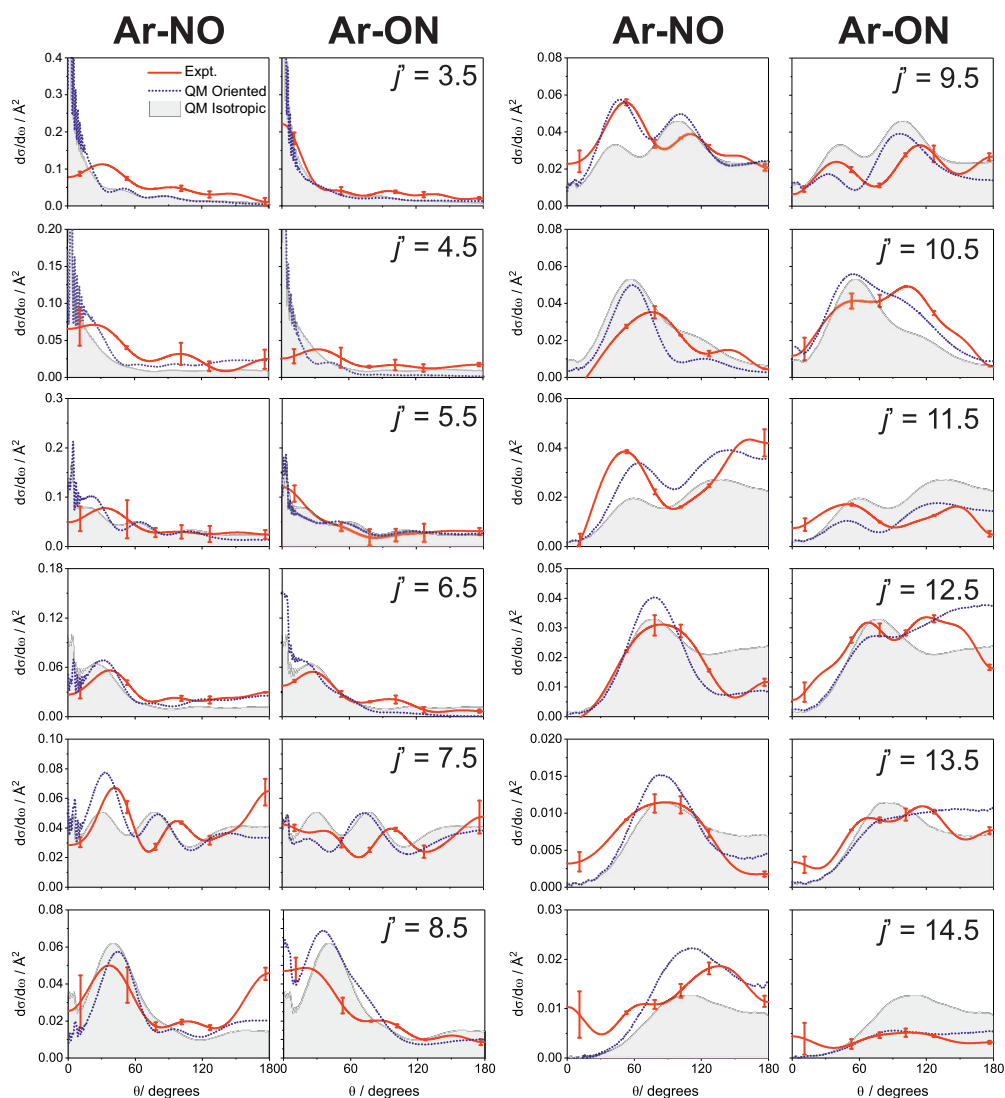


FIG. 5. Experimental fitted (red lines) and QM (blue dashed lines) oriented DCSs for spin-orbit changing collisions of NO with Ar, at a mean collision energy $E_{\text{coll}} = 651 \text{ cm}^{-1}$ and at the static electric field used in the experiments, 9.2 kV cm^{-1} , into the indicated final rotational states, $|j' \Omega' = 1.5, \epsilon' = e\rangle$. DCSs for N-end ($-z$) and O-end ($+z$) collisions of the NO molecule are shown in panels 1 and 3, and 2 and 4, respectively. The QM 'isotropic' DCSs (in the presence of the orienting field) are shaded in grey. Error bars (95% confidence interval) have been calculated from fits to the fast and slow sides of the image and to the total image. The QM data have been averaged over collision energy weighted by a Gaussian of 35 cm^{-1} FWHM.

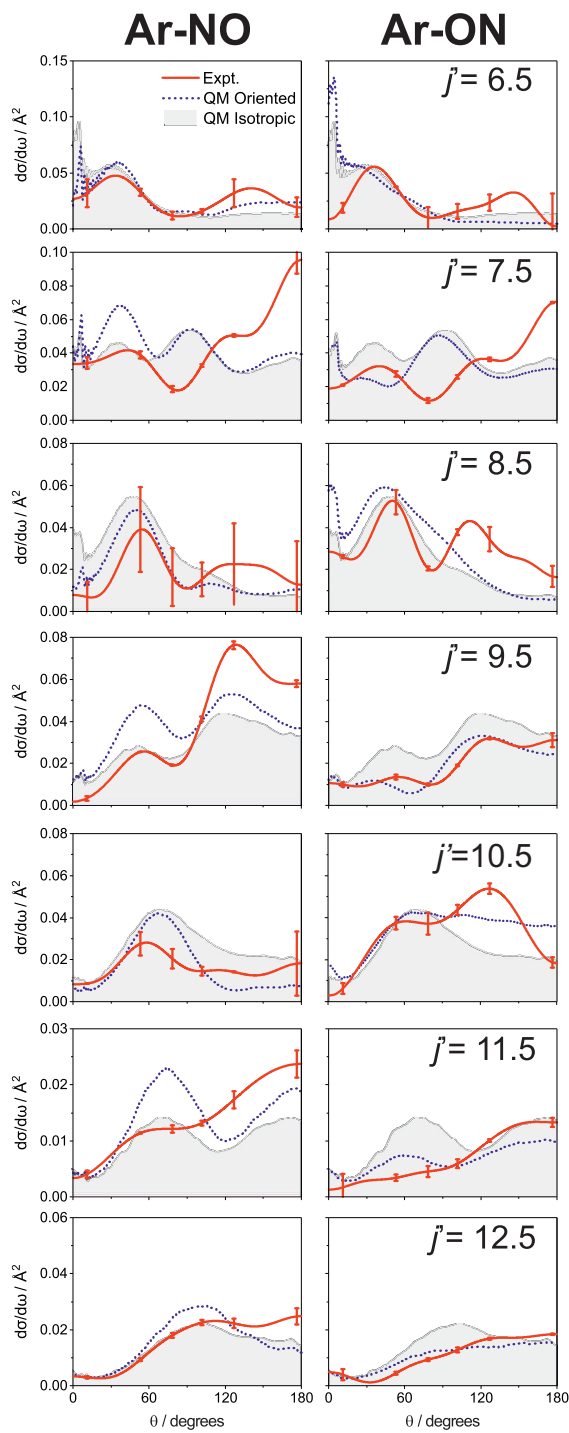


FIG. 6. Same as Fig. 5, but at a mean collision energy $E_{\text{coll}} = 532 \text{ cm}^{-1}$.

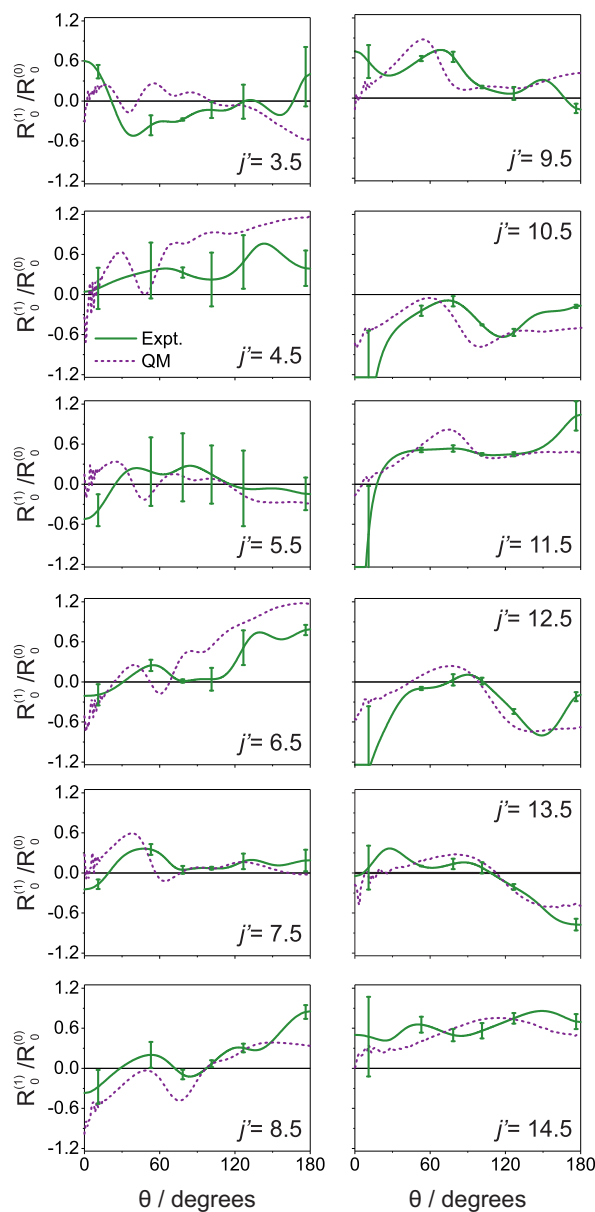


FIG. 7. Experimental (green lines) and CC QM (purple dashed lines) renormalized $R_0^{(1)}(\theta)/R_0^{(0)}(\theta)$ moments for the spin-orbit changing collisions of NO with Ar, at a mean collision energy $E_{\text{coll}} = 651 \text{ cm}^{-1}$ and at the static electric field used in the experiments, 9.2 kV cm^{-1} , into the indicated final rotational states, $|j', \Omega' = 1.5, \epsilon' = e\rangle$. Error bars were calculated by error propagation from the DCSs shown in Fig. 5, and correspond to a 95% confidence interval. The QM data have been averaged over collision energy weighted by a Gaussian of FWHM 35 cm^{-1} .

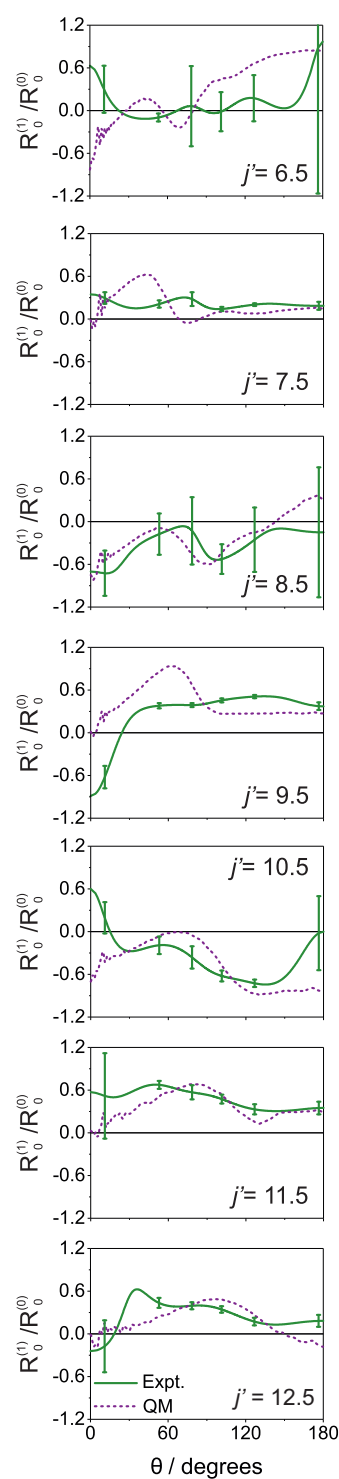


FIG. 8. Same as Fig. 7, but at a mean collision energy $E_{\text{coll}} = 532 \text{ cm}^{-1}$. Error bars, calculated by error propagation from the DCSs in Fig. 6, correspond to a 95% confidence interval.

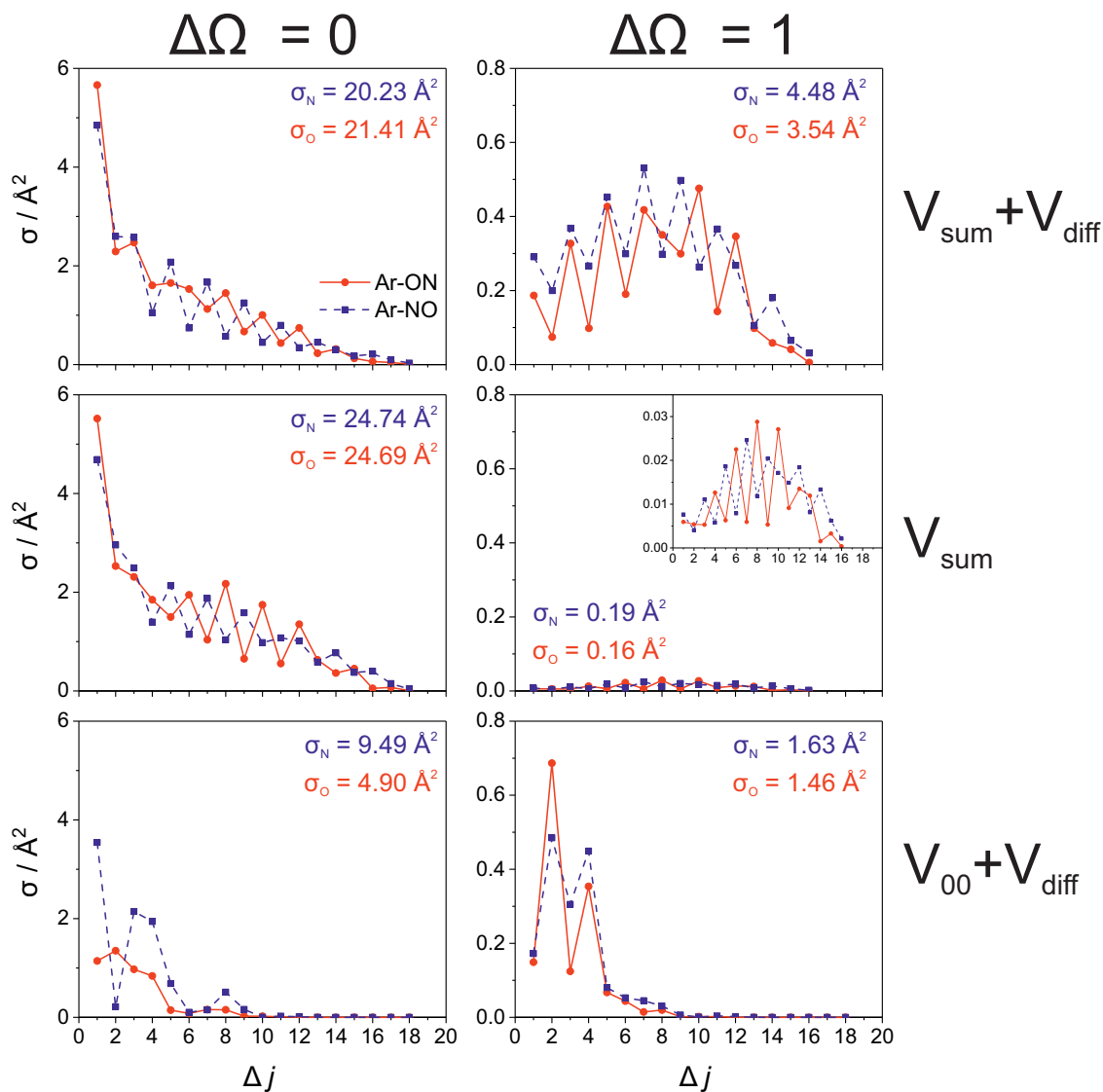


FIG. 9. Theoretical (CC QM) integral cross sections (ICSs) for NO(X) + Ar at a fixed collision energy of $E_{\text{coll}} = 651 \text{ cm}^{-1}$. SO conserving transitions (left column) and SO changing (right column) cross sections are resolved into N-end (blue points and dashed lines) and O-end (red points and continuous lines) collisions at the static electric field used in the experiments, 9.2 kV cm^{-1} . The ICSs were obtained on the full PESs of Alexander^{6,7} (top row), on the V_{sum} PES only (middle row) and on $V_{00} + V_{\text{diff}}$ only (bottom row). The total cross sections, summed over Δj , are also given in each panel.

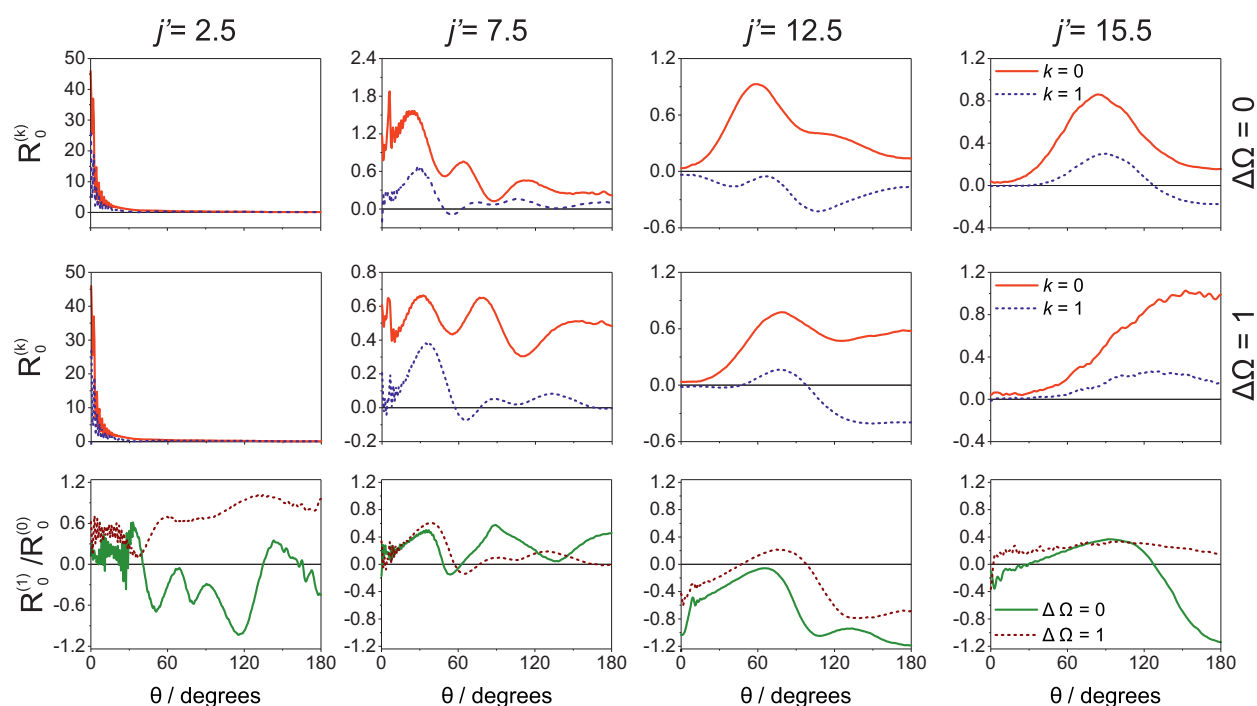


FIG. 10. QM r -PDDCSs for spin-orbit conserving (top row) and spin-orbit changing (middle row) transitions at a fixed collision energy of $E_{\text{coll}} = 651 \text{ cm}^{-1}$ and at the static electric field used in the experiments, 9.2 kV cm^{-1} . The $R_0^{(0)}(\theta)$ and $R_0^{(1)}(\theta)$ moments are shown by red (continuous) and blue (dashed) lines, respectively, in the top two rows of the figure. The bottom row shows the renormalized (1,0) moments, $R_0^{(1)}(\theta)/R_0^{(0)}(\theta)$, for the spin-orbit conserving (green lines) and changing (maroon dashed lines) transitions, respectively. The results correspond to the final e Λ -doublet levels for the rotational states $j' = 2.5, 7.5, 12.5$ and 15.5 (from left to right).